Temperature dependent Al-induced crystallization of amorphous Ge thin films on SiO2 substrates

doi: 10.1016/j.jcrysgro.2013.03.031

Temperature dependent Al-induced crystallization of amorphous Ge thin films on SiO_2 substrates

Kaoru Toko[a], Naoki Fukata[b], Koki Nakazawa[a], Masashi Kurosawa[c], Noritaka Usami[d], Masanobu Miyao[c], and Takashi Suemasu[a]

[a] *Institute of Applied Physics, University of Tsukuba, Tsukuba, Ibaraki 305-8573, Japan*

[b] *National Institute for Materials Science, Namiki, Tsukuba, 305-0044, Japan*

[c] *Department of Electronics, Kyushu University, Motooka, Fukuoka 819-0395, Japan*

[d] *Institute of Materials Research, Tohoku University, Sendai, Miyagi 980-8577, Japan*

Keywords: A1.Crystal orientation, A2.Solid phase crystallization, B1.Polycrystalline films; B2.Semiconducting germanium

High-quality crystalline Ge thin-films on low-cost glass substrates are desired to reduce the fabrication cost of high-efficiency tandem solar cells. We applied an Al-induced crystallization technique to amorphous-Ge films (50-nm thickness) on SiO_2 glass substrates. The annealing temperature of the sample strongly influenced the grain size and the crystal orientation in the grown polycrystalline Ge layers: low annealing temperatures resulted in large grains and high (111)-orientation fractions. As a result, annealing at 325 $^{\circ}$C provided 98% (111)-oriented grains with average diameters of 30-μm. Moreover, the grown Ge layers could be used as an epitaxial template for chemical vapor deposition. This large-grained Ge film on a SiO_2 substrate appears promising for use as a Ge light-absorbing layer, as well as an epitaxial buffer layer for group III-V compound semiconductors.

1. Introduction

Germanium has been used in the bottom cell of high-efficiency tandem solar cells because of its desirable characteristics, such as its narrow band gap (0.66 eV), large absorption coefficient (~10^4 cm^{-1} at 1.1 eV), and good lattice matching to group III-V compound semiconductors (0.1% lattice mismatch with GaAs) [1]. However, bulk Ge substrates are extremely expensive, which has limited their application to special uses, such as in tandem solar cells for space satellites. One promising approach to reducing fabrication cost is substituting the bulk Ge substrate with a high-quality Ge thin film on a low-cost glass substrate. Here, a low-temperature process (< 550 °C) is required to avoid softening the glass substrate. Considering the absorption coefficient of Ge, the optimum thickness of the Ge layer is calculated to be approximately 3-μm. In order to be able to draw photoexcited carriers to the bottom and top electrodes, the grain size in the Ge layer should be larger than 3-μm in diameter, because grain boundary scattering quenches the photoexcited carriers. Specifically, a polycrystalline Ge (poly-Ge) layer works almost as well as a single-crystal Ge substrate if the grain size is sufficiently large and the crystallinity of each grain is sufficiently high. A promising technique for forming large-grained group III-V compound semiconductors for the middle or top cells is epitaxial growth from each grain of the bottom Ge layer [2]. Regarding the crystal orientation, (111)-oriented Ge is favorable for forming nanowires, which dramatically enlarge the light-absorbing area [3, 4]. Many researchers have developed

advanced growth techniques: solid-phase crystallization (SPC) [5-7], metal-induced SPC [8-10], laser annealing [11-13], and chemical vapor deposition (CVD) [14]. However, the resulting Ge layers consist of small, submicron grains, with nearly random orientations.

Aluminum-induced crystallization (AIC) is a metal-induced SPC technique developed for amorphous-Si (a-Si) films on glass substrates [15-23]. CVD of Si layers onto the AIC-Si thin film is a promising approach to fabricating low-defect, large-grained Si layers on glass substrates [24, 25]. However, AIC of amorphous Ge (a-Ge) had been difficult to accomplish [26-29]. Recently, we realized Ge-AIC by preparing thin Ge and Al layers (50-nm thickness) and optimizing the thickness of the AlO_x interfacial layer (~1 nm) [30]. This resulted in preferentially (111)-oriented (~68%) poly-Ge films with relatively large-grains (5-μm diameters). In this paper, the (111)-orientation fraction and the grain size are dramatically improved by lowering the annealing temperature. Moreover, we demonstrate the usability of the Al-induced crystallized Ge (AIC-Ge) films as an epitaxial template for large-grained active Ge layers.

2. Experimental procedure

The preparation of the Al and Ge layers on quartz glass (SiO_2) substrates was carried out at room temperature using a radio-frequency magnetron sputtering method. The deposition times were 2.5 minutes for Al and 2.2 minutes for Ge, respectively. Between the

two deposition cycles, the Al films were exposed to air for 5 minutes to form native AlO_x layers, in order to form a diffusion control layer. The thicknesses of the Al and a-Ge layers were selected to be 50 nm each, because this thickness is favorable for the AIC growth of a-Ge [30]. Finally, the samples were annealed at 325-400 $^{\circ}$C in N_2 for 1-100 h. The surface morphologies of the Ge layers were observed by Nomarski optical microscopy and scanning electron microscopy (SEM). The Raman spectra were recorded using a Jobin Ivon Raman microprobe system, with an Ar^+ laser (514.5 nm) excitation in a backscattering geometry. θ-2θ x-ray diffraction (XRD) measurements were performed using a Rigaku SmartLab system with a Ge monochromator at a wavelength of 1.54 Å. The grain size and crystal orientation were evaluated by electron backscattered diffraction (EBSD) measurement. Prior to the EBSD measurement, the aluminum and oxide layers on the Ge layers were etched using an HF solution (HF: 1.5%) for one minute.

3. Results and Discussion

Figs. 1(a) shows the expected schematic diagrams of the respective crystallization stages, that is, Ge diffusion into Al, Ge lateral growth, and layer exchange. Each diagram corresponds to its respective Nomarski optical micrograph in Fig. 1(b). These micrographs show the back surface of the sample observed through the transparent quartz substrate. The annealing temperature is 375 $^{\circ}$C. These micrographs suggest that the Ge atoms diffuse to the

back surface, grow laterally, and cover the entire substrate during the annealing. The Raman spectra in Fig. 1(c) show the appearance of a large peak after annealing. This peak, at around 295 cm^{-1}, originates from the vibration mode of Ge-Ge bonds, indicating the crystallization of the Ge layer through the layer exchange process. These results typically demonstrate the completion of AIC of a-Ge on a quartz glass substrate.

The EBSD measurement statistically characterizes the crystal orientation of the AIC-Ge, as a function of the annealing temperature (400 °C, 375 °C, 350 °C, and 325 °C). The lower the annealing temperature, the longer the annealing time required for completion of the AIC: (a) 1 h (400 °C), (b) 10 h (375 °C), (c) 30 h (350 °C), and (d) 100 h (325 °C). The crystal orientation maps along the normal (*z*) and in-plane (*x*) directions relative to the sample surfaces are respectively shown in Figs. 2(a)-2(d) and Figs. 2(e)-2(h). We can estimate the grain size from the in-plane orientation maps, because the in-plane crystal directions are different among the respective grains. The orientation maps in Fig. 2 clearly indicate that the orientation and grain size of the AIC-Ge layers strongly depend on the annealing temperature: a lower annealing temperature results in a dominant (111) orientation and a larger grain size in the AIC-Ge layers.

The EBSD analysis is used to derive the area-fractions of the (111) orientation; the average grain size from the EBSD maps is shown in Figs. 2(a)-2(h). The result is shown in Fig. 3(a). By definition, the (111) fraction contains planes with tilt that is within 10^{o} of the

exact (111) plane. Fig. 3(a) clearly indicates that both the (111) fraction and the grain size increase with decreasing annealing temperature. As a result, the (111) fraction is as high as 98% and the grain size is as large as 30-μm diameter for an annealing temperature of 325 °C. These values are the highest among those previously reported for poly-Ge layers on amorphous substrates in low-temperature processes [5-14]. In our previous work on AIC-Ge annealed at 410 °C [30], the (111) fraction and the grain size were limited to 68% and 5 μm, respectively. Therefore, we can conclude that lowering the annealing temperature is very important for enhancing the quality of the poly-Ge films in this AIC technique.

Next we discuss the annealing temperature dependence of the growth morphology. Ge nucleation models are illustrated in Fig. 3(b). In the AIC of Si, it has been reported that Si nucleation occurs when the Si concentration in the Al saturates at a level above the solubility limit [15,17,19,20]. In particular, Sarikov *et al*. clarified that the supersaturation level of Al with Si becomes higher when the annealing temperature is lowered [19]. This mechanism should be the same for the AIC of Ge. During annealing, Ge atoms gradually diffuse into the Al layer through the interfacial AlO_x layer. When the supersaturation level is low, the Ge concentration saturates in the bulk Al before the Ge atoms reach the SiO_2 surface. Because Ge nucleation occurs homogeneously in the bulk Al, the orientation becomes random as shown in Fig. 3(b). In contrast, when the supersaturation level is high, Ge atoms can reach the SiO_2 surface without supersaturation occurring, and without homogeneous nucleation occurring in

126 the bulk Al. In the case of heterogeneous nucleation, the interfacial energy determines the
127 preferential orientation of the nuclei [19, 31]. Because the (111) plane has the lowest
128 interfacial energy in the diamond structure, (111)-oriented Ge nucleation occurs
129 heterogeneously on the SiO_2 surface [32]. Therefore, the preference for the (111) orientation
130 increases as the annealing temperature decreases. For the AIC technique, the initial nucleation
131 density determines the grain size because lateral growth stops when the growth fronts collide
132 [20]. Because a higher supersaturation level causes a lower nucleation rate [17,19], using a
133 low annealing temperature results in a large-grained poly-Ge film.

134 We investigated epitaxial thickening of Ge on the AIC-Ge (grown at 350 °C) using the
135 CVD technique to confirm that this AIC-Ge can be used as an epitaxial template for advanced
136 materials and nanowires. In the CVD, we employed a GeH_4 gas source and kept the sample
137 substrate at 450 °C. A 200-nm thick Ge layer was grown on the AIC-Ge film. The SEM and
138 EBSD images of the CVD-thickened sample surface are shown in Figs. 4(a) and 4(b),
139 respectively. The CVD layer clearly shows predominantly (111) orientation. This result
140 indicates CVD epitaxial growth of the Ge layer on the AIC-Ge film, because conventional
141 CVD-Ge layers without AIC-Ge templates consist of small grains with random orientations
142 [14].

143 XRD measurements are performed to evaluate the epitaxial relationship between the
144 CVD-Ge and AIC-Ge layers. Fig. 5(a) shows the XRD patterns taken from θ-2θ

measurements for the samples before and after CVD thickening. In both patterns, sharp peaks are observed at around 27^{o}, which corresponds to the Ge (111) plane. This figure clearly shows that the CVD thickening strongly enlarges the Ge (111) peak, and other peaks do not appear. A reciprocal space map was obtained around the Ge (111) plane and is shown in Fig. 5(b). A wide contour is observed in the reciprocal space map, which reflects the tilted (111) planes. The maximum tilt angle is calculated to be 12 degrees. This contour has only a single peak, which suggests that the orientation of the AIC-Ge and CVD-Ge layers is the same, due to homoepitaxial growth. The lattice constant of the Ge layer is calculated to be 5.658 Å from the peak position, a value that is almost the same as the relaxed Ge lattice constant (5.66 Å). Therefore, we have demonstrated the usability of this AIC-Ge thin film on an insulator as an epitaxial template for the CVD-Ge layer. It is expected that epitaxial growth of other advanced materials and unidirectionally aligned nanowires is possible using this technique.

4. Conclusions

We have investigated the Al-induced crystallization (AIC) of an a-Ge film (50-nm thickness) on an insulator. The crystallization of the a-Ge layer occurred through the layer-exchange process. We found that the annealing temperature of the sample strongly influenced the grain size and crystal orientation in the grown Ge layers: a lower annealing temperature yielded larger grains and a higher (111)-orientation fraction. Annealing at 325 $^{\circ}$C

increased the grain size to up to 30-μm in diameter and the (111)-orientation fraction to up to 98%. Moreover, the grown Ge layers proved suitable for use as an epitaxial template for chemical vapor deposition (CVD). This large-grained Ge layer on an insulator holds promise for use as a Ge light-absorbing layer and as an epitaxial buffer layer, not only for group III-V compound semiconductors, but also for nanowires and other advanced materials.

Acknowledgements

This work was partially supported by a Grant-in-Aid for Scientific Research from the Ministry of Education, Culture, Sport, Science, and Technology in Japan.

References

[1] R.R. King, D.C. Law, K.M. Edmondson, C.M. Fetzer, G.S. Kinsey, H. Yoon, R.A. Sherif, N.H. Karam, Appl. Phys. Lett. **90** (2007) 183516.

[2] M.G. Mauk, J.R. Balliet, B.W. Feyock, J. Cryst. Growth **250** (2003) 50.

[3] N. Fukata, K. Sato, M. Mitome, Y. Bando, T. Sekiguchi, M. Kirkham, J. I. Hong, Z. L. Wang, R. L. Snyder, ACS Nano **4** (2010) 3807.

[4] E.P. M. Bakkers, J. van Dam, S. De Franceschi, L.P. Kouwenhoven, M. Kaiser, M. Verheijen, H. Wondergem, P. van der Sluis, Nature Materials **3** (2004) 769.

[5] C.Y. Tsao, J.W. Weber, P. Campbell, P.I. Widenborg, D. Song, M.A. Green, Appl. Surf. Sci. **255** (2009) 7028.

[6] A.F. Khan, M. Mehmood, A.M. Rana, T. Muhammad, Appl. Surf. Sci. **256** (2010) 2031.

[7] K. Toko, I. Nakao, T. Sadoh, T. Noguchi, M. Miyao, Solid-State Electron. **53** (2009) 1159.

[8] H. Kanno, K. Toko, T. Sadoh, M. Miyao, Appl. Phys. Lett. **89** (2006) 182120.

[9] J.H. Park, P. Kapur, K.C. Saraswat, H. Peng, Appl. Phys. Lett. **91** (2007) 143107.

[10] K. Toko, H. Kanno, A. Kenjo, T. Sadoh, T. Asano, M. Miyao, Appl. Phys. Lett. **91** (2007) 042111.

[11] H. Watakabe, T. Sameshima, H. Kanno, M. Miyao, Thin Solid Films **508** (2006) 315.

[12] W. Yeh, H. Chen, H. Huang, C. Hsiao, J. Jeng, Appl. Phys. Lett. **93** (2008) 094103.

[13] K. Sakaike, S. Higashi, H. Murakami, S. Miyazaki, Thin Solid Films **516** (2008) 3595.

193 [14] M. Tada, J.H. Park, J.R. Jain, K.C. Saraswat, J. Electrochem. Soc. **156** (2009) D23.

194 [15] O. Nast, T. Puzzer, L.M. Koschier, A.B. Sproul, S.R. Wenham, Appl. Phys. Lett. **73**

195 (1998) 3214.

196 [16] Y. Sugimoto, N. Takata, T. Hirota, K. Ikeda, F. Yoshida, H. Nakashima, H. Nakashima,

197 Jpn. J. Appl. Phys. **44** (2005) 4770.

198 [17] J. Schneider, A. Sarikov, J. Klein, M. Muske, I. Sieber, T. Quinn, H.S. Reehal, S. Gall, W.

199 Fuhs, J. Cryst. Growth **287** (2006) 423.

200 [18] J.Y. Wang, Z.M. Wang, and E.J. Mittemeijer, J. Appl. Phys. **102** (2007) 113523.

201 [19] A. Sarikov, J. Schneider, J. Berghold, M. Muske, I. Sieber, S. Gall, W. Fuhs, J. Appl.

202 Phys. **107** (2010) 114318.

203 [20] B.I. Birajdar, T. Antesberger, B. Butz, M. Stutzmann, E. Spiecker, Scripta Materialia **66**

204 (2012) 550.

205 [21] M. Kurosawa, N. Kawabata, T. Sadoh, M. Miyao, Appl. Phys. Lett. **95** (2009) 132103.

206 [22] M. Jung, A. Okada, T. Saito, T. Suemasu, N. Usami, Appl. Phys. Express **3** (2010)

207 095803.

208 [23] M. Kurosawa, K. Toko, N. Kawabata, T. Sadoh, M. Miyao, Solid-State Electron. **60**

209 (2011) 7.

210 [24] I. Gordon, L. Carnel, D.V. Gestel, G. Beaucarne, J. Poortmans, Thin Solid Films **516**

211 (2008) 6984.

212 [25] B.R. Wu, S.Y. Lo, D.S. Wuu, S.L. Ou, H.Y. Mao, J.H. Wang, R.H. Horng, Thin Solid
213 Films **520** (2012) 5860.
214 [26] F. Katsuki, K. Hanafusa, M. Yonemura, T. Koyama, M. Doi, J. Appl. Phys. **89** (2001)
215 4643.
216 [27] S. Hu, A.F. Marshall, P.C. McIntyre, Appl. Phys. Lett. **97** (2010) 082104.
217 [28] Z. Wang, J. Wang, L. Jeurgens, E. Mittemeijer, Phys. Rev. B **77** (2008) 1.
218 [29] S. Peng, D. Hu, D. He, Appl. Surf. Sci. **258** (2012) 6003.
219 [30] M. Kurosawa, N. Kawabata, T. Sadoh, M. Miyao, ECS J. Solid State Sci. and Tech. **1**
220 (2012) 144.
221 [31] C. Spinella, S. Lombardo, F. Priolo, J. Appl. Phys. **84** (1998) 5383.
222 [32] A.A. Stekolnikov, J. Furthmuller, F. Bechstedt, Phys. Pev. B **65** (2002) 115318.

Fig. 1. (a) Schematic structures of the expected growth stage during AIC of a-Ge. (b) Nomarski optical micrographs of the back surface of the sample annealed at 375 °C for 0 h, 2 h, and 10 h. (c) Raman spectra before and after annealing. The peak at 295 cm^{-1} corresponds to the Ge-Ge vibration mode.

Fig. 2. EBSD images of the AIC-Ge surfaces after annealing at 400 °C, 375 °C, 350 °C, and 325 °C. (a)-(d) normal (*z*) and (e)-(h) in-plane (*x*) directions with respect to the sample surface. The colors indicate the crystal orientation, according to the inserted color keys.

Fig. 3. (a) The (111)-orientation area-fraction and grain size of the AIC-Ge layers as a function of the annealing time. (b) Schematic model of the temperature-dependent (111)-orientation fraction and grain size: (111)-oriented nuclei are generated at the Ge/SiO_2 interface.

Fig. 4. (a) SEM and (b) EBSD images of the thickened Ge layer grown on the AIC-Ge template.

Fig. 5. XRD characterization of the thickened Ge layer grown on the AIC-Ge template. (a) XRD patterns obtained by θ–2θ measurements before and after CVD-thickening and (b)

reciprocal space mapping taken around the Ge (111) reflection.

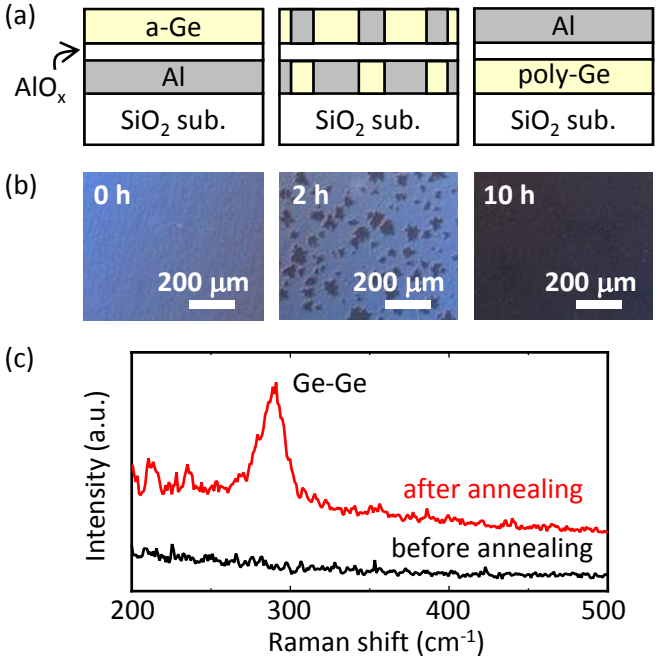

Figure 1 K. Toko

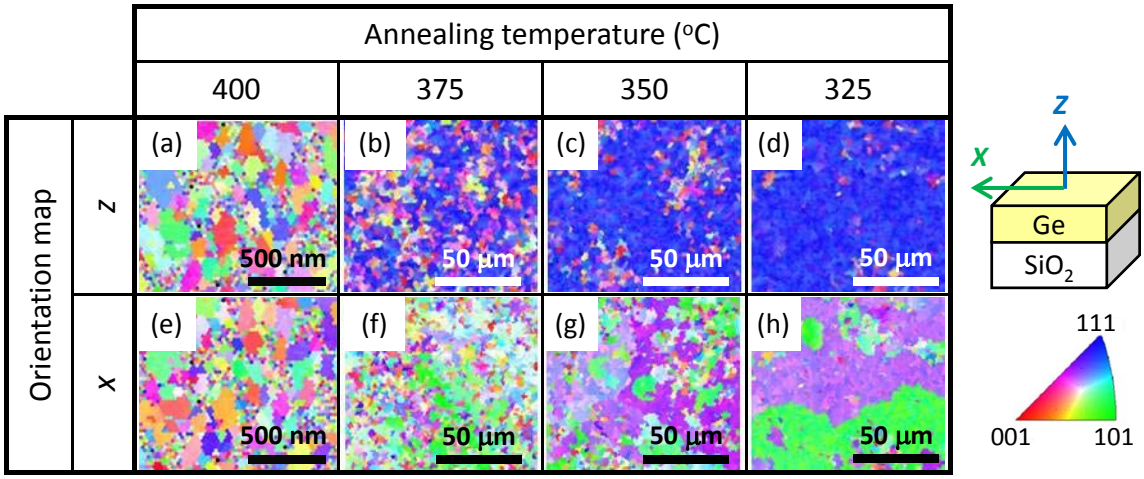

Figure 2 K. Toko

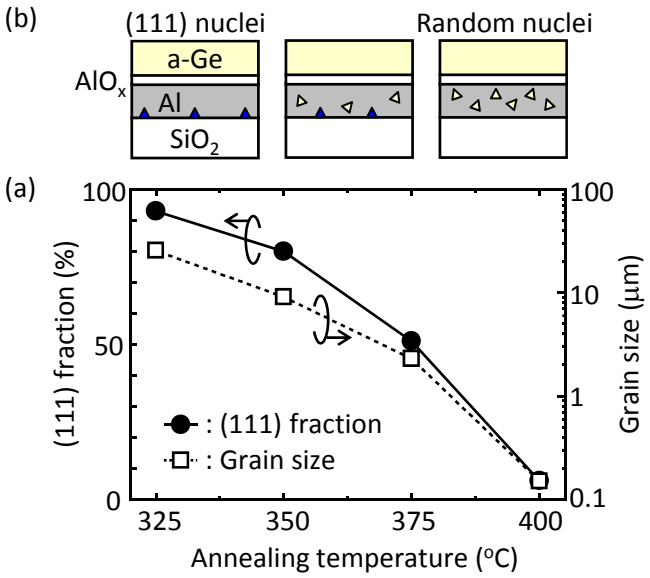

Figure 3 K. Toko

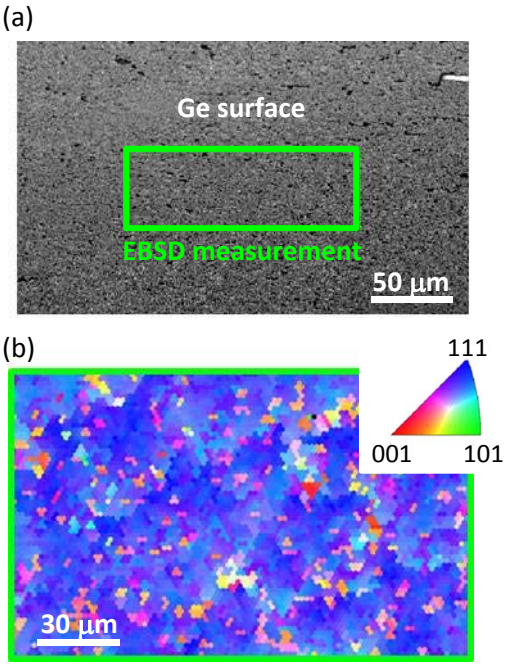

Figure 4 K. Toko

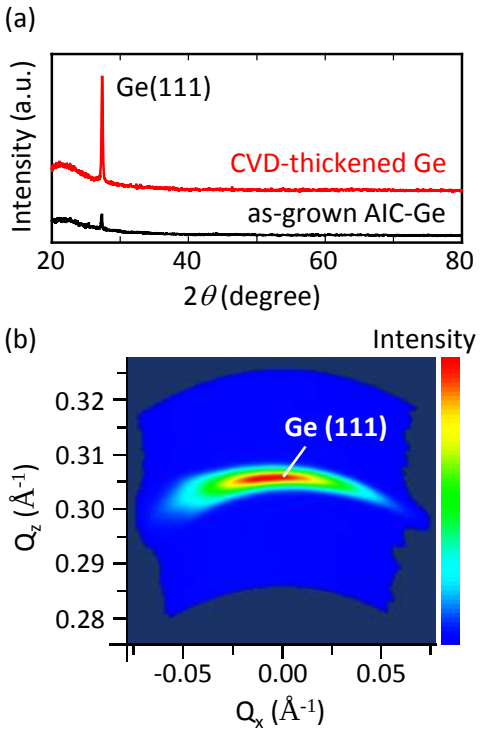

Figure 5 K. Toko